Intracellular vesicle trafficking plays an essential role in mitochondrial quality control

Mike Gerards[a,b], Giuseppe Cannino[a,†], Jose M. González de Cózar[a], and Howard T. Jacobs[a,c,*]
[a]Faculty of Medicine and Life Sciences and Tampere University Hospital, FI-33014 University of Tampere, Finland;
[b]Maastricht Center for Systems Biology (MaCSBio), Maastricht University, 6229 ER Maastricht, The Netherlands;
[c]Institute of Biotechnology, FI-00014 University of Helsinki, Finland

ABSTRACT **The *Drosophila* gene products Bet1, Slh, and CG10144, predicted to function in intracellular vesicle trafficking, were previously found to be essential for mitochondrial nucleoid maintenance. Here we show that Slh and Bet1 cooperate to maintain mitochondrial functions. In their absence, mitochondrial content, membrane potential, and respiration became abnormal, accompanied by mitochondrial proteotoxic stress, but without direct effects on mtDNA. Immunocytochemistry showed that both Slh and Bet1 are localized at the Golgi, together with a proportion of Rab5-positive vesicles. Some Bet1, as well as a tiny amount of Slh, cofractionated with highly purified mitochondria, while live-cell imaging showed coincidence of fluorescently tagged Bet1 with most Lysotracker-positive and a small proportion of Mitotracker-positive structures. This three-way association was disrupted in cells knocked down for Slh, although colocalized lysosomal and mitochondrial signals were still seen. Neither Slh nor Bet1 was required for global mitophagy or endocytosis, but prolonged Slh knockdown resulted in G2 growth arrest, with increased cell diameter. These effects were shared with knockdown of betaCOP but not of CG1044, Snap24, or Syntaxin6. Our findings implicate vesicle sorting at the *cis*-Golgi in mitochondrial quality control.**

Monitoring Editor
Thomas D. Fox
Cornell University

Received: Oct 30, 2017
Accepted: Jan 11, 2018

INTRODUCTION

Mitochondria are multifunctional, dynamic organelles responsible for hundreds of biochemical reactions. Although the most important function of mitochondria is cellular energy conservation through oxidative phosphorylation (OXPHOS), they are also involved in many other processes, including regulation of calcium levels, biogenesis of iron–sulfur clusters, sterol, steroid, and phospholipid biosynthesis, and regulation of apoptosis (for review see Smith *et al.*, 2012). A healthy mitochondrial population is crucial for cellular survival and functioning, and this depends on several quality control processes (Suliman and Piantadosi, 2016). Defects in these processes prevent the clearance of dysfunctional mitochondrial components, leading to the accumulation of mitochondrial damage and eventually to metabolic failure, with pathological consequences (Cenini and Voos, 2016; Liang and Kobayashi, 2016; Romanello and Sandri, 2016). Mitochondrial quality control mechanisms include the mitochondrial unfolded protein response (UPRmt; Haynes *et al.*, 2013), the cycle of mitochondrial fusion and fission (Wai and Langer, 2016), mitophagy (Lemasters, 2014; Hamacher-Brady and Brady, 2016), sequestration into endosomes (Hammerling *et al.*, 2017), and the recently described degradation of mitochondrial-derived vesicles (MDVs; Soubannier *et al.*, 2012; Lemasters, 2014; Sugiura *et al.*, 2014).

The UPRmt is activated upon mitochondrial stress caused by the accumulation of unfolded or misfolded proteins. The mitochondria possess several chaperones and proteases that unfold and then

This article was published online ahead of print in MBoC in Press (http://www.molbiolcell.org/cgi/doi/10.1091/mbc.E17-10-0619) on January 17, 2018.

The authors declare no conflict of interest.

†Present address: CNR Institute of Neuroscience and Department of Biomedical Sciences, University of Padua, 35131 Padua, Italy.

Author contributions: M.G. codesigned the study, performed the experiments, and cowrote the manuscript; G.C. performed biochemical analyses of mitochondrial function; J.G.de C. performed subcellular fractionation and Western blotting; H.T.J. codesigned the study, compiled the figures, and cowrote the manuscript.

*Address correspondence to: Howard T. Jacobs (howard.t.jacobs@uta.fi).

Abbreviations used: ER, endoplasmic reticulum; FCCP, carbonyl cyanide-4-(trifluoromethoxy)phenylhydrazone; GFP, green fluorescent protein; mtDNA, mitochondrial DNA; RNAi, RNA interference; TMRM, tetramethylrhodamine, methyl ester.

either refold or degrade these misfolded or unfolded proteins. Defects in this process lead to the appearance of protein aggregates and have been associated with spastic paraplegia, ataxia, and neurodegenerative diseases such as Alzheimer's and Parkinson's diseases (Arnould *et al.*, 2015).

Mitochondrial fusion and fission occur continuously, serving to isolate damaged compartments and target them for turnover. When mitochondria are subject to prolonged or extreme stresses, the mitochondrial network can become highly fragmented, leading to clearance of damaged compartments by Parkin-mediated turnover pathways, after which the network can be restored (Ni *et al.*, 2015). Mitophagy has also been proposed to remove damaged mitochondrial DNA (mtDNA) molecules, preventing the production of nonfunctional OXPHOS subunits (Carelli *et al.*, 2015). Additionally, the mitochondrial network can be hyperfused upon transient stress to protect the organelles from unnecessary turnover or possibly to minimize organellar damage by dividing the stress among the population. Defective fusion or fission has been associated with dominant optic atrophy and Charcot–Marie–Tooth disease (Züchner *et al.*, 2004; Amati-Bonneau *et al.*, 2008; Yu-Wai-Man *et al.*, 2009; Ryu *et al.*, 2010; Nguyen *et al.*, 2017).

Recently, a new mechanism for clearance of damaged mitochondrial compartments by MDVs was described (Soubannier *et al.*, 2012). There appear to be multiple subtypes of MDVs involved in different pathways of interorganellar communication and quality maintenance (Sugiura *et al.*, 2014). In one of these, MDVs containing lipids, specific proteins, and protein complexes are released from mitochondria and delivered to multivesicular bodies for targeted degradation. The exact contribution of MDVs to mitochondrial quality control is still unclear, as is the mechanism whereby damaged components are selected for and trafficked into this turnover pathway.

In a genomewide RNA interference (RNAi) screen for factors involved in mtDNA replication or copy-number maintenance, based on the loss of mitochondrial nucleoid signal in *Drosophila* S2 cells (Fukuoh *et al.*, 2014), we previously identified several proteins proposed to be involved in vesicle trafficking. Orthologues of two of these, Bet1 and Slh (homologue of yeast Sly1), are conserved components of the syntaxin 5-SNARE complex (Newman *et al.*, 1990; Dascher *et al.*, 1991; Nichols and Pelham, 1998; Xu *et al.*, 2000; Zhang and Hong, 2001; Yamaguchi *et al.*, 2002), which is required for vesicle trafficking from the ER to the Golgi in the canonical secretory pathway, but has not previously been implicated in mitochondrial functions. A third protein identified in the screen, CG10144, is a *Drosophila* homologue of Vps8, a yeast protein involved in vesicle sorting to lysosomes (Chen and Stevens, 1996). The previous study (Fukuoh *et al.*, 2014) found no evidence for any direct role of these proteins in mtDNA maintenance. We therefore embarked on a wider study to elucidate their roles in mitochondria. Our findings implicate vesicle sorting at the *cis*-Golgi as crucial for mitochondrial quality control, and ultimately also for cell-cycle progression and avoidance of cellular senescence.

RESULTS

Knockdown of Slh or Bet1 impairs mitochondrial function

After verifying the efficacy of RNAi-based knockdown of Slh, Bet1, and CG10144 in *Drosophila* S2 cells (Figure 1A), we retested the effects on mtDNA. Even under conditions of prolonged knockdown (10 d), there was no significant change in mtDNA copy number, as measured by quantitative PCR (Figure 1B). Because this method does not reveal subtle changes in mtDNA integrity or topology, we implemented Southern blots of both undigested and *Pst*1-linearized mtDNA from control and knockdown cells (Figure 1C). Knockdown of the three genes produced no change in the representation of different topological forms of (undigested) mtDNA (Figure 1C, leftmost four lanes) and no appearance of subgenomic fragments following linearization, which would be indicative of deletions, nicking, or replication defects (Figure 1C, rightmost four lanes). To investigate whether these proteins are involved in more general mitochondrial functions, we analyzed several key parameters during knockdown, including mitochondrial respiration (measured by oxygen consumption), membrane potential (based on TMRM fluorescence), cellular content of mitochondria (Mitotracker Green fluorescence), and expression of genes implicated in the mitochondrial unfolded protein response, mtUPR (by quantitative reverse-transcription PCR [qRTPCR]). Over 5 d, knockdown of Slh resulted in decreased mitochondrial respiration (77% of control values), while knockdown of Bet1 or CG10144 had no such effect (Figure 2A). Prolonged Slh knockdown for 10 d produced a further decrease in respiration (55% of control values), whereas the smaller drop in respiration due to Bet1 or CG10144 knockdown still did not reach statistical significance. The decreased mitochondrial respiration due to Slh knockdown was accompanied by increased TMRM fluorescence (Figure 2B) but decreased

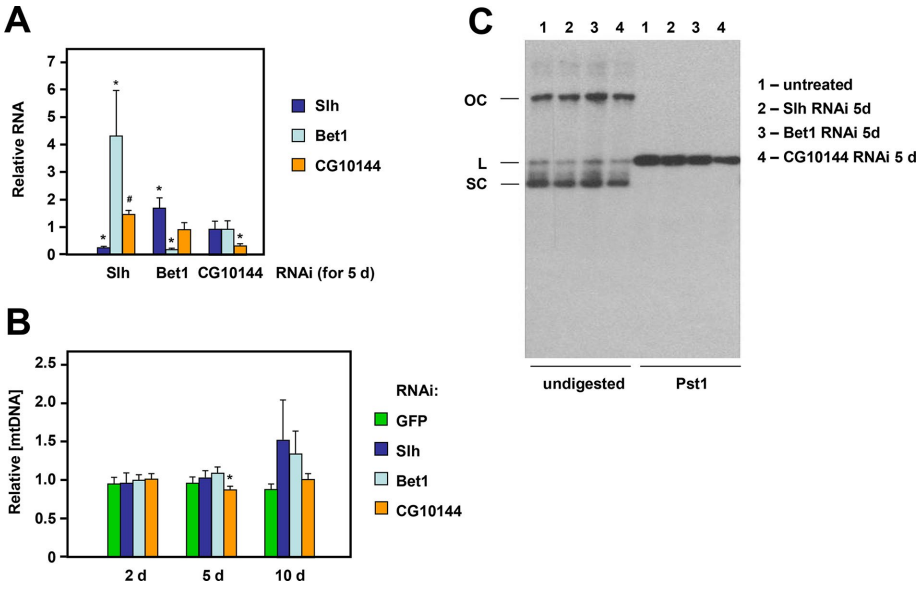

FIGURE 1: Slh, Bet1, or CG10144 knockdown does not affect mtDNA copy number, topology, or integrity. (A) Relative RNA levels of the indicated genes, normalized against RpL32 RNA and then renormalized against the values for untreated S2 cells, and (B) relative mtDNA copy number (based on qPCR), also normalized against the values for untreated S2 cells. Means ± SD, significant differences from control cells (Student's *t* test with Bonferroni correction, $n \geq 4$ biological replicates) denoted by * ($p < 0.01$) and # ($p < 0.05$). (C) Southern blot of mtDNA, ± digestion with *Pst*I, from untreated S2 cells or cells treated with dsRNAs against the indicated genes, for the number of days shown. The main topological forms of mtDNA are indicated as OC (open circles), L (linears), and SC (supercoiled circles).

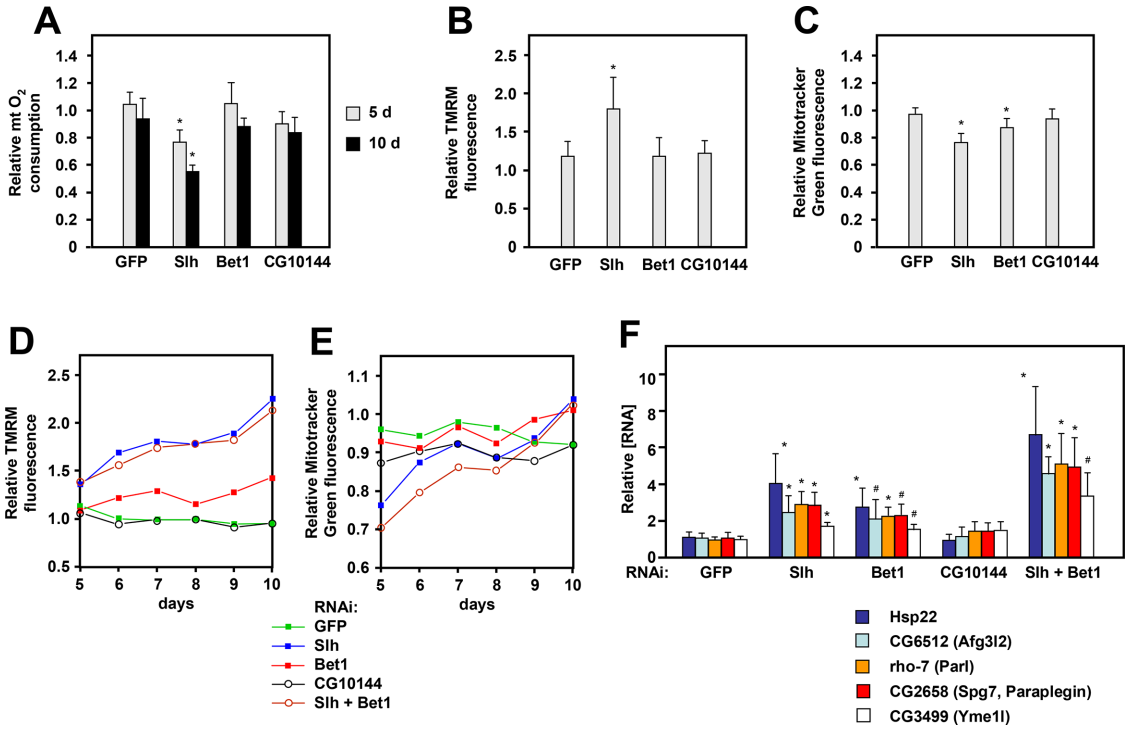

FIGURE 2: Slh knockdown impairs mitochondrial functions. (A) Mitochondrial O_2 consumption, normalized against cell number, (B) TMRM fluorescence per cell, (C) Mitotracker Green fluorescence per cell, (D, E) time course of changes in (D) TMRM fluorescence and (E) Mitotracker Green fluorescence per cell, and (F) relative RNA levels of the indicated genes, normalized against RpL32 RNA; all renormalized against the values for untreated S2 cells, in cells treated with dsRNAs against the indicated genes for the number of days shown. (A–C, F) Means ± SD, significant differences from control cells (Student's *t* test with Bonferroni correction, $n \geq 4$ biological replicates) denoted by * ($p < 0.01$) and # ($p < 0.05$). (D, E) Means of time courses (for source data, including SD and statistical analysis, see Supplemental Table S1); note that *y* axes do not commence at 0.

Mitotracker Green fluorescence per cell (Figure 2C). Knockdown of Bet1 or CG10144 for 5 d had only minor effects on these parameters (Figure 2, B and C). However, prolonged knockdown of Bet1, up to 10 d, also resulted in significantly increased TMRM fluorescence per cell (Figure 2D, Supplemental Table S1), while prolonged knockdown of Slh showed an eventual restoration of the level of Mitotracker Green fluorescence to control values (Figure 2E). The importance of both Slh and Bet1 in mitochondrial functions was further supported by a marked increase in the expression of Hsp22 and various mitochondrial proteases (Figure 2F), which are considered to be indicators of mitochondrial proteotoxic stress (Chan and McQuibban, 2013; Haynes *et al.*, 2013; Morrow *et al.*, 2016) Their expression was increased further by combined knockdown of Slh and Bet1 (Figure 2F), although effects on membrane potential and mitochondrial content were similar to those produced by knockdown of Slh alone (Figure 2, D and E). Finally, knockdown of either Slh or Bet1 produced a marked increase in the expression of the other (Figure 1A), while CG10144 expression was almost unchanged upon knockdown of Slh or Bet1 or vice versa (Figure 1A). These results indicate an important role for the SNARE-binding protein Slh and the SNARE protein Bet1 in maintaining mitochondrial functions and suggest that they may act in a common pathway, while CG10144 likely has a different role.

Bet1 and Slh localize to the Golgi

To gain more insight into how Bet1 and Slh affect mitochondria, we studied their subcellular localization in *Drosophila* S2 cells, using epitope tagging. The V5 epitope tag did not disturb the targeting of previously characterized mitochondrial or cytosolic proteins (Supplemental Figure S1A). However, immunocytochemistry did not convincingly detect colocalization of V5-tagged Bet1 or Slh with mitochondria (Figure 3, A and B, panels a–c and j–l; Table 1). Instead, both proteins were found to colocalize with the *cis*-Golgi marker GM130 (Figure 3, A and B, panels d–f and m–o; Table 1), as well as with approximately half of all vesicles bearing the early endosome marker Rab5 (Figure 3, A and B, panels g–i and p–r; Table 1).

To investigate this issue further, we developed a subcellular fractionation procedure for S2 cell lysates that yields highly purified cytoplasmic (i.e., postmitochondrial) and mitochondrial fractions. Using Western blotting, we then studied the association of Bet1-V5 and Slh-V5 in fractions from transiently transfected cells. The *cis*-Golgi marker GM130 was present in the postmitochondrial (cytoplasmic) fraction, but was undetectable in the highly purified mitochondrial fraction (Figure 3C), whereas Cox4 was abundant in the latter and only faintly visible in the cytoplasmic fraction when overexposed (Figure 3C). However, probing with the V5 antibody revealed that some Bet1-V5 routinely cofractionated with highly purified mitochondria, as did a tiny amount of Slh-V5 (Figure 3C). Note that overexpression of V5-tagged Bet1 or Slh produced no change in the intracellular distribution or morphology of mitochondria (Supplemental Figure S1B), and labeling patterns were homogeneous across many cells, arguing that the observed colocalizations were not due to an overexpression artifact.

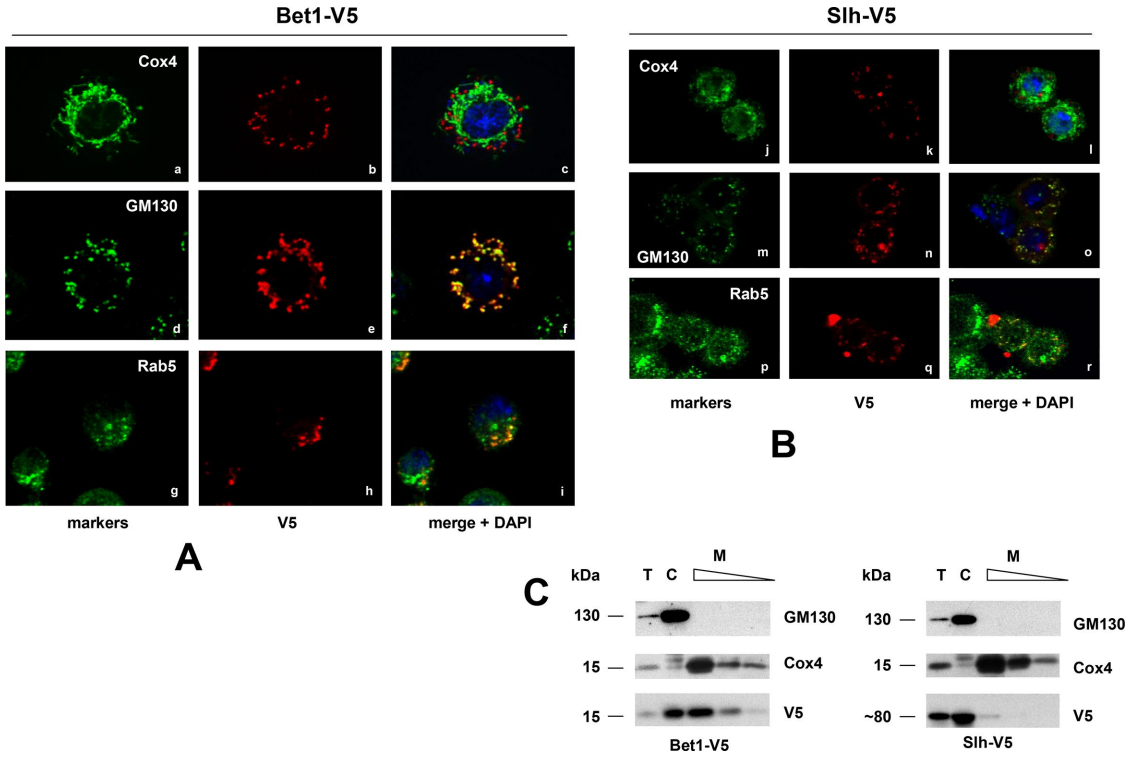

FIGURE 3: Bet1 and Slh localize to multiple cellular membranes, based on epitope tagging. Immunocytochemistry for the indicated markers, Cox4 (mitochondria), GM130 (*cis*-Golgi), Rab5 (early endosomes), in cells transiently transfected with (A) Bet1-V5 or (B) Slh-V5, as shown. Images were optimized on the microscope for brightness and contrast, but have not been manipulated in any other way, apart from the addition of panel labels as referred to in the text. (C) Western blots of protein extracts from Bet1-V5 and Slh-V5 transfected cells, probed as indicated. T—total cellular extract, 20 µg, C, cytoplasmic (postmitochondrial) fraction, 20 µg; M, highly purified mitochondrial fraction, shown at increasing dilution (20, 10, 4 µg). Extrapolated molecular weights (kDa) of the detected bands, inferred from the migration of molecular weight markers, shown alongside. Note that *Drosophila* Cox4, like that of mammals, runs on SDS–12% PAGE gels at ~15 kDa; its N-terminal processing is unknown. Slh-V5 is ~74 kDa but appears to migrate closer to 80 kDa on SDS–PAGE. Blot images were optimized for brightness and contrast, cropped, and resized for clarity, but not manipulated in any other way.

Transfected construct	Bet1-V5	Slh-V5
(i) Cells costained for V5 and Rab5		
Number of individual cells analyzed	24	20
Number of V5-positive structures per cell	18 ± 5	22 ± 9
Number of Rab5-positive structures per cell	34 ± 11	29 ± 8
% of V5-positive structures also positive for Rab5	96 ± 11	83 ± 16
% of Rab5-positive structures also positive for V5	52 ± 10*	60 ± 14*
(ii) Cells costained for V5 and GM130		
Number of individual cells analyzed	24	16
Number of GM130-positive structures per cell	25 ± 5	28 ± 4
% of V5-positive structures also positive for GM130	100	100
% of GM130-positive structures also positive for V5	100	100
(iii) Cells costained for V5 and Cox4		
Number of individual cells analyzed	23	21
Number of V5-positive structures per cell	26 ± 6	26 ± 8
% of V5-positive structures also positive for Cox4	0	0

*Not significantly different, Student's *t* test with Bonferroni correction, $p > 0.05$.

TABLE 1: Subcellular localization of Bet1 and Slh based on epitope tagging and marker colocalization.

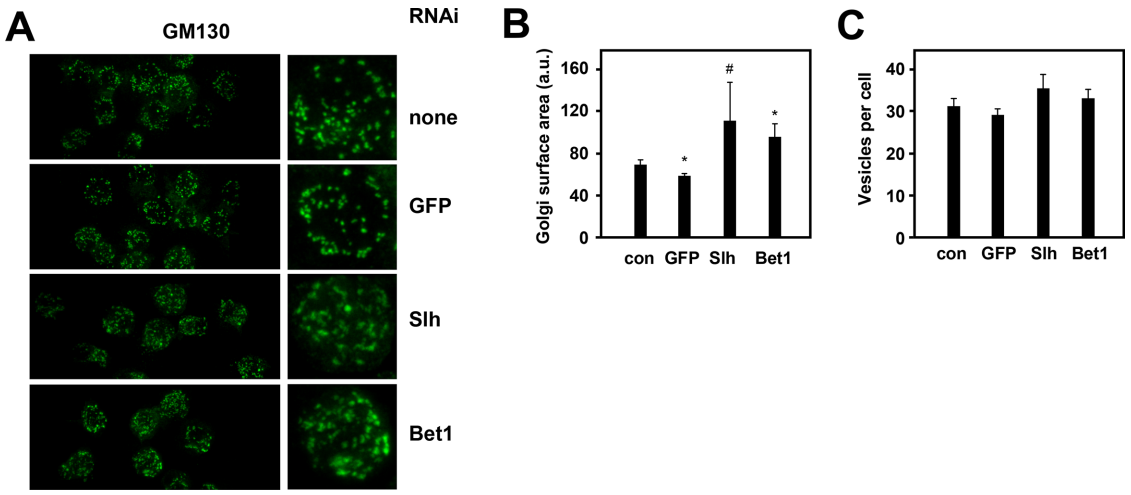

FIGURE 4: Bet1 and Slh knockdown result in Golgi enlargement. (A) Immunocytochemistry for GM130 (*cis*-Golgi marker) of cells knocked down by dsRNA treatment for 5 d, targeted on the indicated genes, with zoomed image showing typical cells. (B) Surface area, calculated using ImageJ software, and (C) number of Golgi vesicles per cell, based on such images (≥60 cells in each case). Means ± SD; #, * indicate statistically significant differences from control (con) cells (Student's *t* test with Bonferroni correction, $p < 0.05$ and $p < 0.01$, respectively). Images were optimized on the microscope for brightness and contrast, but have not been manipulated in any other way, apart from the addition of panel labels as referred to in the text. Note that an ~60% increase in surface area represents a twofold change in volume.

Taken together, these findings indicate that both proteins are located in close proximity to the Golgi, and in structures that also contain endocytic and mitochondrial components, although not the *cis*-Golgi marker GM130. Because Bet1-V5 and Slh-V5 were both found to colocalize mostly with GM130, we investigated the effect of their knockdown on Golgi structure. In both cases, there was a significant increase in Golgi size (Figure 4, A and B), while the number of Golgi structures was unchanged (Figure 4, A and C). The finding is consistent with both proteins playing a role in Golgi function, though their knockdown does not lead to complete loss of Golgi.

Slh is required for the colocalization of mitochondria, lysosomes, and Bet1

The identity and subcellular distribution of Bet1 and Slh (Figure 3) suggest involvement in vesicle sorting, whereas the effects of their knockdown (Figure 2) indicate, in addition, that they are needed to prevent mitochondrial proteotoxic stress, that is, the accumulation of damaged mitochondrial components. Taken together, these observations suggest that Bet1/Slh-associated vesicles could be involved in the turnover of mitochondria-derived material, and specifically in its selective targeting to lysosomes for degradation. To test this idea, we used live-cell imaging of cells expressing a Bet1-BFP (blue fluorescent protein) fusion protein, combined with staining of mitochondria and lysosomes respectively with Mitotracker Green and Lysotracker Red (Figure 5), In control cells, a majority of the structures positive for both Mitotracker Green and Lysotracker Red were also positive for Bet1-BFP (Figure 5, A, panels a–d, and B). In contrast, knockdown of Slh almost completely abolished this colocalization (Figure 5, A, panels e–h, and B). Colocalization of Mitotracker Green and Lysotracker Red was still observed to an extent similar to that in control cells, but these structures were no longer positive for Bet1-BFP, which was seen in separate foci. The pattern of colocalization of Bet1-BFP with Lysotracker Red and Mitotracker Green was not disturbed upon CG10144 knockdown (Supplemental Figure S2). These results support the idea that Bet1 and Slh together play a role in the interaction of mitochondria and lysosomes and, taking account of loss of mitochondrial functionality when either is knocked down, support the idea that this influences the specificity of mitochondrial quality control or turnover.

Slh is not required for mitophagy or endocytosis

The observation that Slh is required for the normal intracellular localization of mitochondrial material associated with lysosomes suggests that it may be required for one of the previously studied mitochondrial turnover pathways. To test whether Slh is needed for the well-characterized process of mitophagy, we treated control and Slh-knockdown cells with the uncoupler FCCP (5 μM), which induces global mitophagy, as revealed by the complete colocalization of mitochondria and lysosomes within 2 h of such treatment. Slh knockdown made no difference to this process: complete colocalization of Mitotracker Green and Lysotracker Red signal was observed, both in control and in Slh knockdown cells (Figure 6A).

Following the recent identification of an alternate pathway of mitochondrial turnover involving sequestration into endosomes (Hammerling *et al.*, 2017), we also tested whether Bet1 and Slh are needed for endocytosis, using an assay based on uptake of the non-membrane-permeant pH-sensitive dye pHrodo Red Dextran. Knockdown of Slh or Bet1 resulted in no systematic disruption of the endocytic pathway, based on this assay (Figure 6B).

Knockdown of Bet1 and Slh produces growth arrest and increased cell size

After 5 d of knockdown, fewer cells were present in wells transfected with double-stranded RNA (dsRNA) against Bet1 or Slh, compared with control wells (Figure 7A). To study whether knockdown of Bet1 and Slh leads to a decreased growth rate or to increased cell death, the total number of cells was monitored in each well over 10 d of culture. While a clear increase in cell number was evident for control S2 cells and for cells knocked down using an inert dsRNA targeted

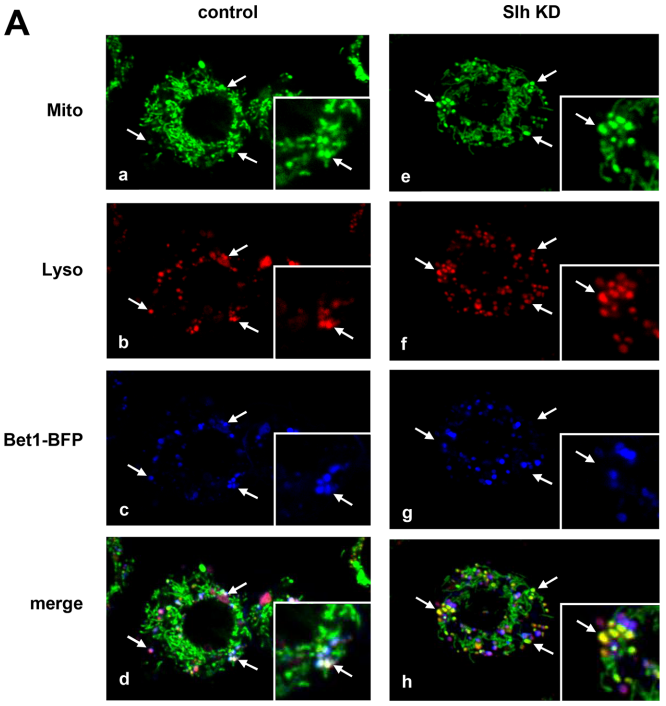

FIGURE 5: Slh is required for Bet1 coassociation with lysosomal and mitochondrial components. (A) Representative live-cell images of cells transfected with Bet1-BFP, either alone (control S2 cells, con, panels a–d) or with concomitant knockdown of Slh (panels e–h), costained with Lysotracker Red and Mitotracker Green, together with (inset) zoomed images at higher magnification. White arrows indicate vesicles positive for Mitotracker Green and Lysotracker Red, which, in control cells, but not Slh knockdown cells, were mostly positive for Bet1-GFP. Images were optimized on the microscope for brightness and contrast, but have not been manipulated in any other way, apart from the addition of panel labels and arrows as referred to here and in the text. (B) Quantitation (%) of structures costained with Mitotracker Green and Lysotracker Red, which were also positive for Bet1-BFP, based on inspection of all visibly fluorescent structures in eight cells of each class analyzed. con, control S2 cells transfected with Bet1-BFP; Slh KD, cells also knocked down for Slh. * denotes a statistically significant difference, $p < 0.001$, Student's *t* test.

against GFP, cell number did not change substantially after Bet1 or Slh was knocked down (Figure 7A). FACS analysis of propidium iodide–stained cells showed that significantly more cells were in G2 phase after 10 d of Slh knockdown than for control cells, indicating a disturbed cell cycle (Figure 7B). The accumulation of cells in G2 was accompanied by an increase in cell size (Figure 7, C and D). Note that an increase in cell diameter of 45% equates to a trebling of cell volume. Knockdown of Bet1 again produced similar but quantitatively less dramatic effects, while knockdown of CG10144 had no effect on cell growth, size, or cell-cycle status (Figure 7, A–C). These results indicate that deficiency of Bet1 or Slh (but not CG10144) leads to cell growth arrest, predominantly in the G2 phase of the cell cycle, with concomitantly increased cell size.

Because Slh and Bet1 have previously been inferred to function in protein secretion (Bard *et al.*, 2006), we tested whether RNAi against other genes known to be involved in vesicle trafficking in the secretory pathway would produce the same effects on mitochondrial proteostasis and cell growth and size as RNAi against Bet1 and Slh. Prolonged knockdown of βCOP, which mediates vesicle transport from the ER to the *cis*-Golgi, had an effect similar to that seen with Slh knockdown (Figure 8, A–D; compare with Figures 7A, 2F, and 7, C and D, respectively), but knockdown of SNAP-24 and Syx6, both of which function in post-Golgi vesicle trafficking (Niemeyer and Schwarz, 2000; Malsam and Söllner, 2011) did not (Figure 8, A–D).

DISCUSSION

Bet1 and Slh, proteins already known to function in the secretory pathway, were previously identified in a genomewide RNAi screen for novel mtDNA replication factors (Fukuoh *et al.*, 2014). Here we showed that they are not directly involved in mtDNA metabolism, but localized at the Golgi, where they appear to function unexpectedly in mitochondrial quality control. The Golgi is considered as the central clearinghouse of the cell, allowing cross-talk between the secretory, endosomal, and autophagic machinery. Here we extend this concept to mitochondria, providing evidence that vesicle trafficking at the Golgi influences mitochondria and may act as a surveillance system for defective mitochondrial components.

Slh and Bet1 cooperate to maintain mitochondrial quality

Bet1 and Slh, *Drosophila* homologues of proteins of the syntaxin 5-SNARE complex, were found to colocalize in S2 cells with Golgi marker GM130, as expected from previous studies showing that they are required for protein secretion (Bard *et al.*, 2006), consistent with their canonical role in other organisms. Unexpectedly, RNAi-induced Slh deficiency led to progressively decreased mitochondrial content, accompanied by decreased mitochondrial respiration and increased per-cell TMRM fluorescence, usually considered indicative of mitochondrial membrane potential. We note that, despite the increase in cell size (Figure 7C), when the increased TMRM fluorescence (Figure 2, B and D) is normalized against mitochondrial content (Figures 2C and 7E), it remains consistently above control levels.

In addition, Slh knockdown caused increased expression of genes mediating mitochondrial proteotoxic stress, notably the major proteases (m-AAA, i-AAA, and rho-7) and the stress-induced chaperone Hsp22, implicating Slh in the maintenance of mitochondrial protein quality. Bet1 knockdown produced similar, though less drastic effects, partially additive with those of Slh knockdown. Decreased respiration, associated with the activation of ATP-dependent intramitochondrial proteases and chaperones, may engender mitochondrial ATP depletion, triggering electrogenic ATP import to maintain mitochondrial functions, and accounting for elevated membrane potential.

Mitochondrial damage accumulation accompanied by decreased mitochondrial content implies a failure of mitochondrial biogenesis, dysregulated mitochondrial turnover, or both. The three-way association of Bet1-BFP with lysosomal and mitochondrial markers, which was disrupted by Slh knockdown, strongly implies turnover as a key target, while leaving open the precise mechanism. One possibility is that Bet1 and Slh are in some way involved in sorting and distinguishing between functional and dysfunctional mitochondrial components, for example, via the recognition of damage markers (McLelland *et al.*, 2014). Slh knockdown was not accompanied by a large increase in colocalization of Lysotracker and Mitotracker signals, implying that the accumulation

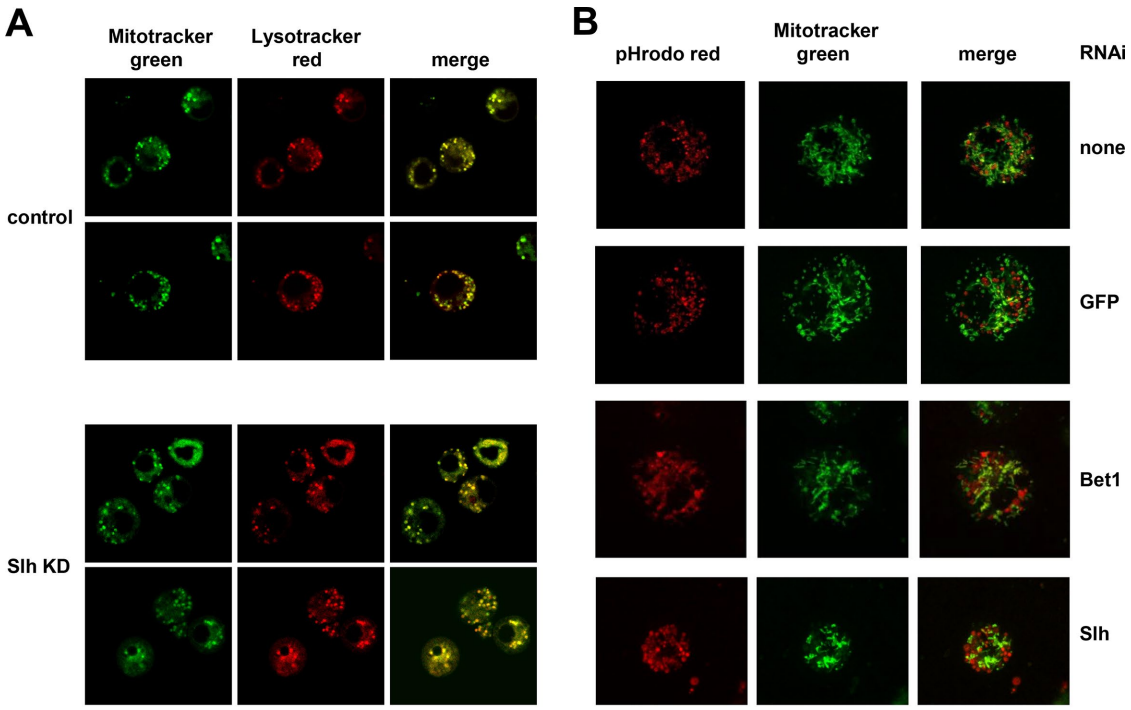

FIGURE 6: Slh is not required for mitophagy or endocytosis. (A) Live-cell imaging of control S2 cells and cells knocked down for Slh, treated for 2 h with 5 μM FCCP and stained with Mitotracker Green and Lysotracker Red. The two probes overlap almost completely in both cases, indicating that Slh knockdown does not interfere with global mitophagy. (B) Visualization of acidified late endosomes and endolysosomes in untreated S2 cells and in cells knocked down for Bet1 or Slh or treated with an inert dsRNA targeted on GFP. Red fluorescence due to the pH-sensitive nonpermeant dextran-conjugated dye pHrodo Red Dextran is visible in all cells.

of mitochondrial damage did not induce an increased amount of turnover, but rather a change in its selectivity. The colocalization of Bet1 with a subset of mitochondria, based both on subcellular fractionation (Figure 3D) and on live-cell imaging (Figure 5), plus its disruption by Slh knockdown (Figure 5), suggests that Bet1 may serve as a tag for mitochondria or MDVs destined for turnover. We hypothesize that Slh may be needed for the docking of Bet1-tagged mitochondrial vesicles at the Golgi and their onward sorting to lysosomes, and that in the absence of this process, mitochondrial interaction with lysosomes is largely nonselective.

The syntaxin-5 SNARE complex and mitochondrial turnover pathways

In mammalian cells, the syntaxin-5 SNARE complex plays a role in autophagy as well as in protein secretion (Renna *et al.*, 2011). This has been attributed to the need for anterograde transport for maturation of lysosomal proteases in the Golgi. In yeast, SNARE and SNARE-binding mutants affecting ER-to-Golgi trafficking, including Bet1 and the Slh homologue Sly1, are deficient in macroautopaghy (Tan *et al.*, 2013), and COPII vesicles have been suggested to supply membranes for autophagosome formation (Tan *et al.*, 2013). However, our data (Figure 6A) indicate clearly that Bet1 and Slh are not required in *Drosophila* S2 cells for global mitophagy, induced by agents that compromise mitochondrial membrane potential (Narendra *et al.*, 2008). The mitochondria-related process disrupted by Bet1 or Slh knockdown in S2 cells must therefore be more specific. The other molecular players involved, and their relationship with the various mitochondrial turnover pathways so far described, remain to be elucidated.

Although Slh and Bet1 are part of the secretory machinery in *Drosophila* (Bard *et al.*, 2006), as in other organisms, our finding that they also colocalize at the Golgi with a proportion of Rab5-positive vesicles suggested that they might also play a role in the endocytic pathway. This raised the possibility that their effect on mitochondria could be indirect, arising, for example, from defective cellular transport of iron. Moreover, a separate study has recently implicated endosomes in an alternative pathway of mitochondrial turnover (Hammerling *et al.*, 2017). MDVs have been shown to associate with the retromer-complex components Vps35and Vps26 (Braschi *et al.*, 2010), which mediate vesicle transport from endosomes to the Golgi. Moreover, Parkinson's disease–associated mutants of *VPS35* are known to produce mitochondrial dysfunction (Wang *et al.*, 2016), and *Vps35* interacts genetically with *parkin* in *Drosophila* (Malik *et al.*, 2015). However, our findings (Figure 6B) demonstrate that Slh and Bet1 are not required for endocytosis in S2 cells. Colocalization with Rab5 is therefore simply a reflection of the role of the Golgi as the cell's central clearinghouse for vesicles in transit.

Why were vesicle-transport genes picked up in a screen for mtDNA maintenance factors?

Exactly why Bet1 and Slh were identified as positives in the original genomewide screen remains unclear. Their knockdown did not affect mtDNA content or integrity (Figure 1). The mechanism by which Pico Green accumulates in mitochondria is not known, but likely requires a mitochondrial membrane potential. Although membrane potential was increased when Slh or Bet1 was knocked down, its hypothesized maintenance by electrogenic ATP import, accompanied by decreased respiration, implies that intramitochondrial pH

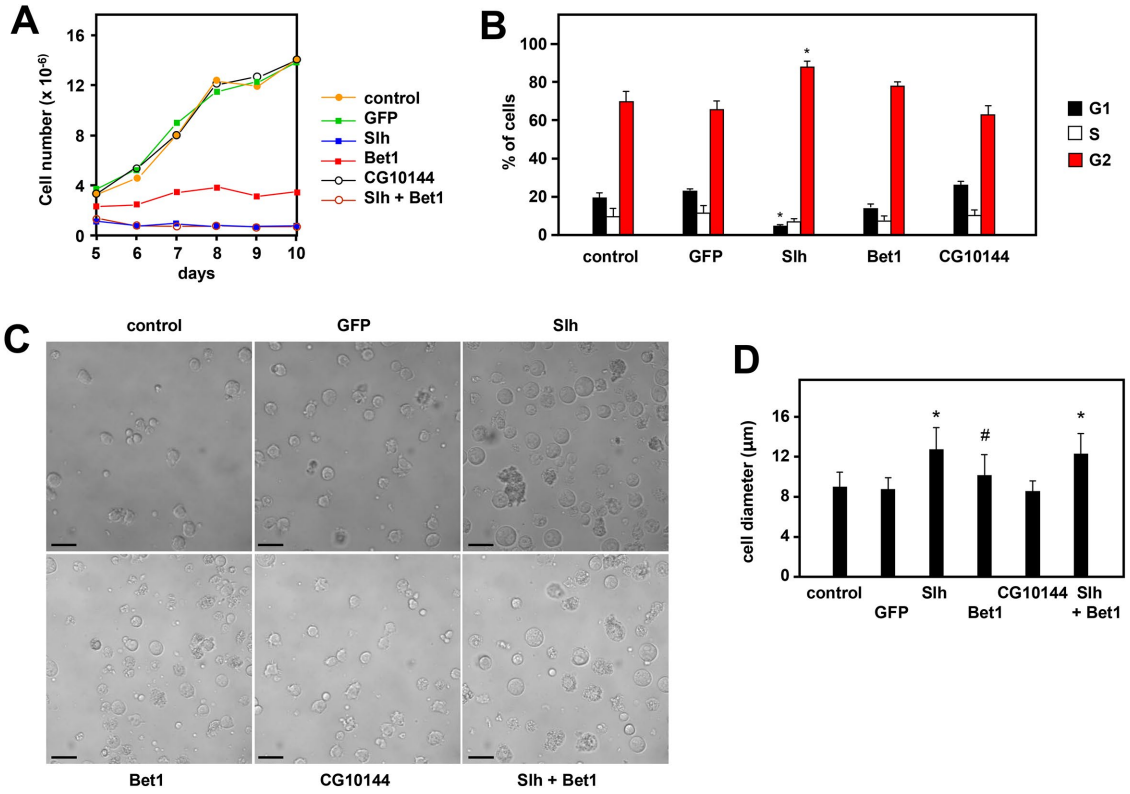

FIGURE 7: Slh and Bet1 knockdown entrains cell growth defects. (A) Growth curves of control S2 cells and cells treated continuously for 10 d, with dsRNAs targeted against the indicated genes, commencing 5 d after transfection. For source data, including SD and statistical analysis, following normalization to cell number on day 5, see Supplemental Table S1. (B) Cell-cycle analysis of control S2 cells and cells knocked down for 10 d by dsRNAs targeted on the indicated genes. (C) Micrographs of control S2 cells and cells after 5 d of treatment with dsRNAs targeted against the indicated genes. Scale bars: 20 µm. (D) Cell diameter of control S2 cells and cells knocked down for the indicated genes (means ± SD of 52 cells of each class). #, * denote significant differences from the corresponding data class of control cells (Student's *t* test with Bonferroni correction, $p < 0.05$ or 0.001, respectively).

may be highly abnormal. This could underlie the loss of Pico Green signal. Alternatively, it may reflect an altered structure of nucleoids caused by proteotoxic stress.

The role of Bet1 and Slh in mitochondrial quality control appears to be shared with at least one other protein involved in vesicle trafficking at the *cis*-Golgi, βCOP (Figure 8). In contrast, proteins that perform other roles in the *trans*-Golgi network, including other SNAREs, such as SNAP-24 and Syx-6, do not appear to be involved in mitochondrial quality maintenance (Figure 8). CG1044 falls into the same category, because its orthologue in yeast, Vps8, is required for the retention of several late-Golgi membrane proteins in the Golgi apparatus, and for the correct sorting of the vacuolar (lysosomal) carboxypeptidase Y (Chen and Stevens, 1996). It is also a member of the CORVET complex, involved in membrane tethering in late endosomes and their interaction with lysosomes (Balderhaar *et al.*, 2013; Solinger and Spang, 2013). This nevertheless raises the similar question of why CG10144 was reproducibly scored as positive in the original screen. Unlike that of Bet1 and Slh, its knockdown produced no effect on any of the mitochondrial parameters tested here.

A link between mitochondrial turnover and senescence

Slh, Bet1, or βCOP knockdown resulted also in G2 proliferation arrest and increased cell size. These are hallmarks of cells undergoing senescence (Rodier and Campisi, 2011) and are also seen in S2 cells disrupted for cell-cycle progression by RNAi against Rho-1 GTPase (Rogers and Rogers, 2008). Links between mitochondrial dysfunction and senescence have been reported previously (Passos *et al.*, 2006; Ziegler *et al.*, 2015), and a recent study showed mitochondrial dysfunction to be causal (Wiley *et al.*, 2016). Intriguingly, this was also associated with a characteristic defect in the secretory pathway. However, we cannot exclude the possibility that the senescence-like phenotype observed here has nothing directly to do with mitochondria. The finding should therefore be treated with caution. Nevertheless, it is clearly an important consequence of Bet1 or Slh knockdown.

The senescence-associated secretory phenotype (SASP) is a common hallmark of senescence that, at least in mammalian cells, involves the secretion of proinflammatory cytokines and other signaling molecules, as well as proteases and other factors that modify the extracellular matrix (Coppé *et al.*, 2010). The underlying mechanisms are poorly understood, but are believed to involve transcriptional changes dictated by chromatin alterations. Here, we induced a senescencelike phenotype by altering the properties of key components of the secretory pathway, rather than producing secretome changes through senescence induction. This supports the idea of senescence as a program rather than a haphazard series of maladaptive changes. Furthermore, it strengthens the view that vesicle sorting at the *cis*-Golgi is a crucial process for maintaining cellular homeostasis and viability, linking both protein secretion and

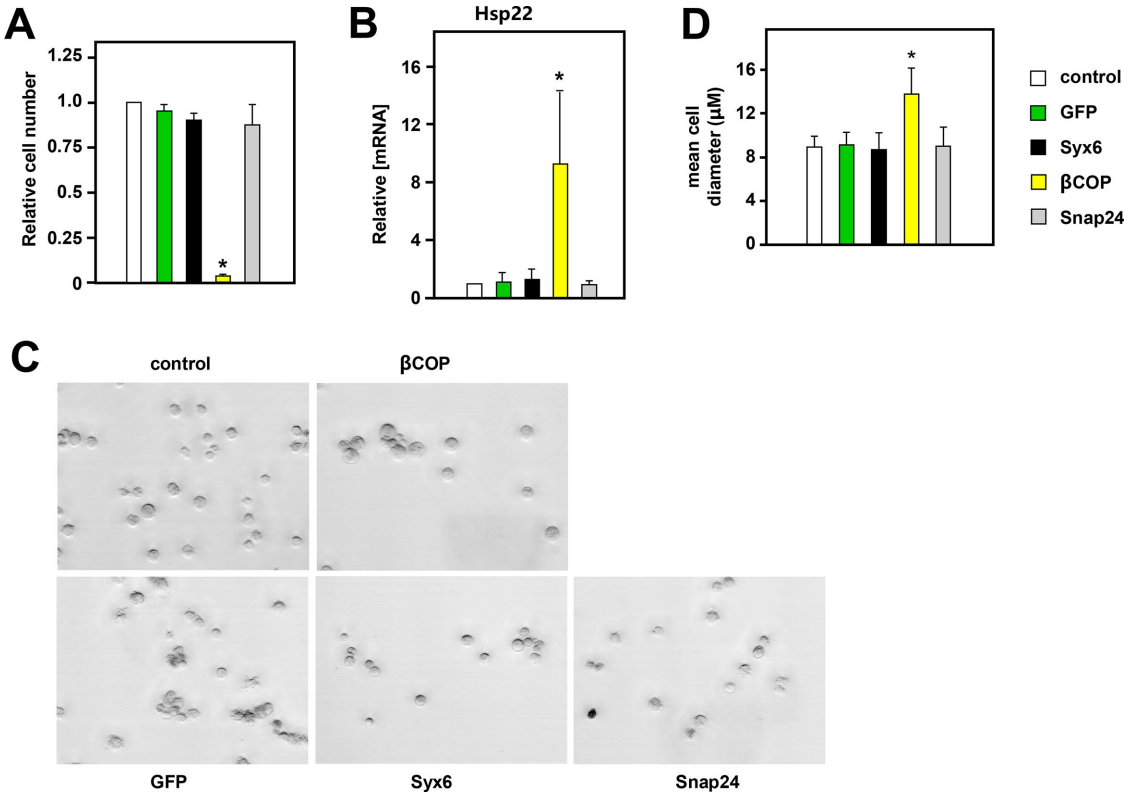

FIGURE 8: Post-Golgi components of the secretory pathway are not needed to maintain mitochondrial quality and cell growth. (A) Relative cell number, compared with control cells, after 5 d of dsRNA treatment against the indicated genes. See also Supplemental Figure S3. (B) Relative level of Hsp22 RNA, normalized against RpL32 RNA and renormalized against the values for untreated S2 cells, after dsRNA treatment against the indicated genes. Because there were so few remaining viable cells after 5 d of βCOP knockdown, RNA levels were assessed after 2 d of knockdown. Means ± SD; significant differences from control cells (Student's *t* test with Bonferroni correction, $n \geq 4$ biological replicates) denoted by * ($p < 0.05$). (C) Micrographs of S2 cells after 5 d of treatment with dsRNAs targeted against the indicated genes. Scale bars: 20 μm. (D) Cell diameter of control (S2) cells and cells knocked down for the indicated genes (means ± SD of 52 cells of each class). * denotes significant differences from the corresponding data class of control cells (Student's *t* test with Bonferroni correction, $p < 0.001$).

mitochondrial damage to cell fate, tissue remodeling, and aging, and suggesting a possible "mitochondrial checkpoint" for cell-cycle progression.

MATERIALS AND METHODS

S2 cell culture

Drosophila S2 cells (Invitrogen) were cultured under standard conditions in Schneider's medium (Sigma). Knockdown was established by treatment with gene-specific dsRNAs. Briefly, dsRNA was generated from T7-labeled PCR products using the MEGAscript T7 transcription kit (Thermo Scientific). For 5-d knockdown experiments, cells were seeded at a density of 10^6 cells/ml and treated with 8 μg/ml dsRNA half an hour after plating. An additional 8 μg/ml dsRNA was added after 3 d. For 10-d knockdown, 10^5 cells/ml were seeded and treated with 2 μg/ml dsRNA half an hour later and with 8 μg/ml dsRNA at days 3, 5, and 8. Additionally, the medium was refreshed after 5 d.

Immunocytochemistry and live-cell imaging

Bet1 and Slh were cloned in frame with the V5-tag in the pMT-V5/His plasmid (Life Technologies), which contains an inducible metallothionein promoter. S2 cells were transfected using FuGene (Promega) according to the manufacturer's instructions. One day after transfection, expression of V5-tagged Bet1 and Slh was induced by adding $CuSO_4$ to a final concentration of 100 μM. Two days after induction, cells were fixed and stained as previously described (Rogers and Rogers, 2008; including plating on ConA) using mouse anti-V5 (Life Technologies) and rabbit anti-COXIV, anti-Rab5, or anti-GM130 (Abcam) as primary antibodies and AlexaFluor 568 goat anti-mouse Immunoglobulin G (IgG) (H+L) and goat anti-rabbit AlexaFluor 488 IgG (H+L) (Life Technologies) as secondary antibodies, and imaged by confocal microscopy. Golgi size and number were calculated using a spot-area calculation with ImageJ. For live-cell imaging of Bet1, the coding sequence of BFP was cloned into the pMT-V5-Bet1 construct between the V5 and the His tags. Cells were transfected with the final construct using FuGene, and expression was induced 1 d after transfection by adding $CuSO_4$ to a final concentration of 100 μM. Two days later, cells were transferred to ConA-coated slides as described previously (Rogers and Rogers, 2008), stained with 25 nM MitoTracker Green FM and 50 nM LysoTracker Red DND-99 (ThermoFisher Scientific), and imaged by confocal imaging.

Intracellular localization by subcellular fractionation and Western blotting

Cells were plated, transfected, and induced as for immunocytochemistry, but on a larger scale (starting from 5×10^7 cells in 100 ml

of medium, transfected with 60 µg of plasmid DNA). Two days after induction, cells were harvested by centrifugation at 1000 × g_{max} for 5 min, with a 1-ml aliquot of cells processed separately as "total cell extract." The latter was washed once with ice-cold phosphate-buffered saline (PBS) and then lysed in 100 µl lysis buffer (50 mM Tris/HCl, 150 mM NaCl, 1 mM EDTA, 1% Triton X-100, pH 7.4) containing 1× cOmplete Protease Inhibitor (Roche). After incubation on ice for 30 min, the sample was centrifuged at 14,000 × g_{max} for 5 min at 4°C, and the supernatant was saved for later analysis. Cell pellets from the main sample were washed once with 20 ml ice-cold PBS, resuspended in 0.1x CHB (4 mM Tris/HCl, 2.5 mM NaCl, 5 mM $MgCl_2$, pH 7.8) on ice, incubated for 6 min, and lysed by 15 strokes of a Dounce homogenizer with a tight-fitting glass pestle. Cell lysis was verified by Trypan blue exclusion, with an additional five strokes if needed. After addition of 1/10 volume of 10x CHB (400 mM Tris/HCl, 250 mM NaCl, 500 mM $MgCl_2$, pH 7.8), homogenates were centrifuged at 200 × g_{max} for 3 min at 4°C. The supernatant was transferred to a fresh tube and centrifugation repeated. The supernatant was then recentrifuged at 1200 × g_{max} for 3 min at 4°C. The pellet was saved, and the supernatant was recentrifuged, with the pellet again saved. The supernatant was recentrifuged twice at 14,000 × g_{max} for 3 min at 4°C, and the final supernatant was processed as the cytoplasmic (postmitochondrial) fraction. The 1200 × g_{max} pellets were washed once with 1x CHB, then combined and resuspended in 250 µl ice-cold 1x CHB, and loaded onto 4-ml sucrose step-gradients consisting of four 1-ml layers (50, 60, 70, and 80% sucrose in 20 mM HEPES/KOH, pH 7.2). After ultracentrifugation at 180,000 × g_{max} for 90 min at 4°C in a swinging-bucket rotor (Beckman SW 60 Ti), highly purified mitochondria were recovered from the 70–80% sucrose interface, diluted up to 2 ml with 225 mM mannitol, 75 mM sucrose, 10 mM Tris/HCl, 1 mM EDTA, and 0.1% bovine serum albumin (BSA), pH 7.6, gently mixed, and then recovered by centrifugation at 14,000 × g_{max} for 10 min at 4°C. The pellet was processed as for the "total cell extract" fraction. Protein concentrations were determined using the Bradford reagent (Sigma), with BSA standards in the same buffer. Aliquots of the protein extracts (see legends) were run on SDS–12% polyacrylamide gels, wet-blotted on nitrocellulose membranes (GE Healthcare), and processed for Western blotting using standard methods, with a reaction buffer containing 0.1% Tween-20 plus 5% nonfat milk except for the final washes. Primary antibodies were against GM130 (Abcam ab30637, rabbit polyclonal, 1:1000 dilution), COX IV (Abcam ab16056, rabbit polyclonal, 1:2000), and V5 (Invitrogen 46-0705, mouse monoclonal, 1:10,000). Secondary antibodies were horseradish peroxidase (HRP) goat anti-rabbit IgG (Vector Laboratories, PI-1000, 1:10,000) and HRP horse anti-mouse IgG (Vector Laboratories, PI-2000, 1:10,000). Signals were detected by chemiluminescence (SuperSignal West Femto Maximum Sensitivity Substrate kit, ThermoFisher Scientific) according to the manufacturer's instructions, with Fujifilm Super RX.

Cell cycle analysis

After 5 or 10 d of dsRNA treatment, cells were collected, pelleted, washed in PBS, and then stained for 30 min on ice in the dark with 500 µl of PI staining solution containing 25 µg/ml propidium iodide, 100 µg/ml RNase A, 0.1% sodium citrate, and 0.1% Triton X-100 (Sigma). After staining, samples were analyzed by flow cytometry (488 nm excitation, >670 nm emission; FL3). The number of cells was plotted against the DNA content at each time point.

mtDNA analysis, RNA isolation, and quantitative PCR

Total DNA isolation and mtDNA copy number analysis by quantitative PCR (qPCR) were performed as previously reported (Fukuoh *et al.*, 2014). mtDNA topology and deletions were assessed by 1D Southern blot analysis on untreated and linearized mtDNA as previously described (Jõers *et al.*, 2013). For transcript analysis, total RNA was isolated and cDNA produced as previously (Jõers *et al.*, 2013). Expression levels were determined by qRTPCR using gene-specific primers. Transcript levels were estimated relative to RPL32.

Measurements of mitochondrial function

Mitochondrial membrane potential and mitochondrial content were measured by flow cytometry after S2 cells were stained with 200 mM TMRM or 40 nM Mitotracker Green FM (ThermoFisher Scientific). Oxygen consumption was measured in living S2 cells with a Clark-type electrode (Hansatech Oxyterm system) as reported previously (Cannino *et al.*, 2012).

Endocytosis and mitophagy assays

All steps were conducted at 25°C. S2 cells were seeded into six-well plates, treated for 5 d with gene-specific dsRNA, and then reseeded on coverslips coated with ConA to facilitate attachment. After 45 min, the medium was removed and replaced with a medium containing 40 nM Mitotracker Green FM (ThermoFisher Scientific). After 30 min incubation, cells were washed three times with normal medium and then incubated with pHrodo Red Dextran 10,000 MW for Endocytosis (ThermoFisher Scientific), 40 µg/ml in PBS, for 15 min, followed by a rapid PBS wash. The coverslip was mounted on a concave microscopy slide containing PBS. After 10 min, cells were imaged by confocal microscopy. To assay global mitophagy, cells were incubated for 2 h with 5 µM FCCP and then processed for live-cell imaging as described above.

Statistical analysis

Comparisons between populations were performed using unpaired two-tailed Student's *t* tests or analysis of variance when more than two samples were compared, with a Bonferroni-corrected post hoc *t* test, as indicated in the figure legends.

ACKNOWLEDGMENTS

The study was funded by the Academy of Finland, the Sigrid Juselius Foundation, and the Tampere University Hospital Medical Research Fund. M.G. was supported by the Dutch Province of Limburg. We thank Tea Tuomela, Outi Kurronen, and Merja Jokela for technical assistance, Brendan Battersby and Anu Suomalainen for useful discussions, and Troy Faithfull for editing the manuscript.

REFERENCES

Amati-Bonneau P, Valentino ML, Reynier P, Gallardo ME, Bornstein B, Boissière A, Campos Y, Rivera H, de la Aleja JG, Carroccia R, *et al.* (2008). OPA1 mutations induce mitochondrial DNA instability and optic "plus" phenotypes. Brain 131, 338–351.

Arnould T, Michel S, Renard P (2015). Mitochondria retrograde signaling and the UPR mt: where are we in mammals? Int J Mol Sci 16, 18224–18251.

Balderhaar HJ, Lachmann J, Yavavli E, Bröcker C, Lürick A, Ungermann C (2013). The CORVET complex promotes tethering and fusion of Rab5/Vps21-positive membranes. Proc Natl Acad Sci USA 110, 3823–3828.

Bard F, Casano L, Mallabiabarrena A, Wallace E, Saito K, Kitayama H, Guizzunti G, Hu Y, Wendler F, DasGupta R, *et al.* (2006). Functional genomics reveals genes involved in protein secretion and Golgi organization. Nature 439, 604–607.

Braschi E, Goyon V, Zunino R, Mohanty A, Xu L, McBride HM (2010). Vps35 mediates vesicle transport between the mitochondria and peroxisomes. Curr Biol 20, 1310–1315.

Cannino G, El-Khoury R, Pirinen M, Hutz B, Rustin P, Jacobs HT, Dufour E (2012). Glucose modulates respiratory complex I activity in response to acute mitochondrial dysfunction. J Biol Chem 287, 38729–38740.
Carelli V, Maresca A, Caporali L, Trifunov S, Zanna C, Rugolo M (2015). Mitochondria: biogenesis and mitophagy balance in segregation and clonal expansion of mitochondrial DNA mutations. Int J Biochem Cell Biol 63, 21–24.
Cenini G, Voos W (2016). Role of mitochondrial protein quality control in oxidative stress-induced neurodegenerative diseases. Curr Alzheimer Res 13, 164–173.
Chan EY, McQuibban GA (2013). The mitochondrial rhomboid protease: its rise from obscurity to the pinnacle of disease-relevant genes. Biochim Biophys Acta 1828, 2916–2925.
Chen YJ, Stevens TH (1996). The VPS8 gene is required for localization and trafficking of the CPY sorting receptor in *Saccharomyces cerevisiae*. Eur J Cell Biol 70, 289–297.
Coppé J, Desprez P, Krtolica A, Campisi J (2010). The senescence-associated secretory ohenotype: the dark side of tumor suppression. Annu Rev Pathol 5, 99–118.
Dascher C, Ossig R, Gallwitz D, Schmitt HD (1991). Identification and structure of four yeast genes (SLY) that are able to suppress the functional loss of YPT1, a member of the RAS superfamily. Mol Cell Biol 11, 872–885.
Fukuoh A, Cannino G, Gerards M, Buckley S, Kazancioglu S, Scialo F, Lihavainen E, Ribeiro A, Dufour E, Jacobs HT (2014). Screen for mitochondrial DNA copy number maintenance genes reveals essential role for ATP synthase. Mol Syst Biol 10, 734.
Hamacher-Brady A, Brady NR (2016). Mitophagy programs: mechanisms and physiological implications of mitochondrial targeting by autophagy. Cell Mol Life Sci 73, 775–795.
Hammerling BC, Najor RH, Cortez MQ, Shires SE, Leon LJ, Gonzalez ER, Boassa D, Phan S, Thor A, Jimenez RE, *et al*. (2017). A Rab5 endosomal pathway mediates Parkin-dependent mitochondrial clearance. Nat Commun 8, 14050.
Haynes CM, Fiorese CJ, Lin YF (2013). Evaluating and responding to mitochondrial dysfunction: the mitochondrial unfolded-protein response and beyond. Trends Cell Biol 23, 311–318.
Jõers P, Lewis SC, Fukuoh A, Parhiala M, Ellilä S, Holt IJ, Jacobs HT (2013). Mitochondrial transcription terminator family members mTTF and mTerf5 have opposing roles in coordination of mtDNA synthesis. PLoS Genet 9, e1003800.
Lemasters JJ (2014). Variants of mitochondrial autophagy: Types 1 and 2 mitophagy and micromitophagy (Type 3). Redox Biol 12, 749–754.
Liang Q, Kobayashi SJ (2016). Mitochondrial quality control in the diabetic heart. J Mol Cell Cardiol 95, 57–69.
Malik BR, Godena VK, Whitworth AJ (2015). VPS35 pathogenic mutations confer no dominant toxicity but partial loss of function in *Drosophila* and genetically interact with parkin. Hum Mol Genet 24, 6106–6117.
Malsam J, Söllner TH (2011). Organization of SNAREs within the Golgi stack. Cold Spring Harb Perspect Biol 3, a005249.
McLelland GL, Soubannier V, Chen CX, McBride HM, Fon EA (2014). Parkin and PINK1 function in a vesicular trafficking pathway regulating mitochondrial quality control. EMBO J 33, 282–295.
Morrow G, Le Pécheur M, Tanguay RM (2016). *Drosophila melanogaster* mitochondrial Hsp22: a role in resistance to oxidative stress, aging and the mitochondrial unfolding protein response. Biogerontology 17, 61–70.
Narendra D, Tanaka A, Suen DF, Youle RJ (2008). Parkin is recruited selectively to impaired mitochondria and promotes their autophagy. J Cell Biol 183, 795–803.
Newman AP, Shim J, Ferro-Novick S (1990). BET1, BOS1, and SEC22 are members of a group of interacting yeast genes required for transport from the endoplasmic reticulum to the Golgi complex. Mol Cell Biol 10, 3405–3414.
Nguyen M, Boesten I, Hellebrekers DME, Mulder-den Hartog NM, de Coo IFM, Smeets HJM, Gerards M (2017). Novel pathogenic SLC25A46 splice-site mutation causes an optic atrophy spectrum disorder. Clin Genet 91, 121–125.
Ni HM, Williams JA, Ding WX (2015). Mitochondrial dynamics and mitochondrial quality control. Redox Biol 4, 6–13.
Nichols BJ, Pelham HR (1998). SNAREs and membrane fusion in the Golgi apparatus. Biochim Biophys Acta 1404, 9–31.
Niemeyer BA, Schwarz TL (2000). SNAP-24, a *Drosophila* SNAP-25 homologue on granule membranes, is a putative mediator of secretion and granule–granule fusion in salivary glands. J Cell Sci 113, 4055–4064.
Passos JF, von Zglinicki T, Saretzki G (2006). Mitochondrial dysfunction and cell senescence: cause or consequence? Rejuvenation Res 9, 64–68.
Renna M, Schaffner C, Winslow AR, Menzies FM, Peden AA, Floto RA, Rubinsztein DC (2011). Autophagic substrate clearance requires activity of the syntaxin-5 SNARE complex. J Cell Sci 124, 469–482.
Rodier F, Campisi JJ (2011). Four faces of cellular senescence. Cell Biol 192, 547–556.
Rogers SL, Rogers GC (2008). Culture of *Drosophila* S2 cells and their use for RNAi-mediated loss-of-function studies and immunofluorescence microscopy. Nat Protoc 3, 606–611.
Romanello V, Sandri M (2016). Mitochondrial quality control and muscle mass maintenance. Front Physiol 6, 422.
Ryu SW, Jeong HJ, Choi M, Karbowski M, Choi C (2010). Optic atrophy 3 as a protein of the mitochondrial outer membranes induces mitochondrial fragmentation. Cell Mol Life Sci 67, 2839–2850.
Smith RA, Hartley RC, Cochemé HM, Murphy MP (2012). Mitochondrial pharmacology. Trends Pharmacol Sci 33, 341–352.
Solinger JA, Spang A (2013). Tethering complexes in the endocytic pathway: CORVET and HOPS. FEBS J 280, 2743–2757.
Soubannier V, McLelland GL, Zunino R, Braschi E, Rippstein P, Fon EA, McBride HM (2012). A vesicular transport pathway shuttles cargo from mitochondria to lysosomes. Curr Biol 22, 135–141.
Sugiura A, McLelland GL, Fon EA, McBride HM (2014). A new pathway for mitochondrial quality control: mitochondrial-derived vesicles. EMBO J 33, 2142–2156.
Suliman HB, Piantadosi CA (2016). Mitochondrial quality control as a therapeutic target. Pharmacol Rev 68, 20–48.
Tan D, Cai Y, Wang J, Zhang J, Menon S, Chou HT, Ferro-Novick S, Reinisch KM, Walz T (2013). The EM structure of the TRAPPIII complex leads to the identification of a requirement for COPII vesicles on the macroautophagy pathway. Proc Natl Acad Sci USA 110, 19432–19437.
Wai T, Langer T (2016). Mitochondrial dynamics and metabolic regulation. Trends Endocrinol Metab 27, 105–117.
Wang W, Wang X, Fujioka H, Hoppel C, Whone AL, Caldwell MA, Cullen PJ, Liu J, Zhu X (2016). Parkinson's disease-associated mutant VPS35 causes mitochondrial dysfunction by recycling DLP1 complexes. Nat Med 22, 54–63.
Wiley CD, Velarde MC, Lecot P, Liu S, Sarnoski EA, Freund A, Shirakawa K., Lim HW, Davis SS, Ramanathan A, *et al*. (2016). Mitochondrial dysfunction induces senescence with a distinct secretory phenotype. Cell Metab 23, 303–314.
Xu D, Joglekar AP, Williams AL, Hay JC (2000). Subunit structure of a mammalian ER/Golgi SNARE complex. J Biol Chem 275, 39631–39639.
Yamaguchi T, Dulubova I, Min SW, Chen X, Rizo J, Südhof TC (2002). Sly1 binds to Golgi and ER syntaxins via a conserved N-terminal peptide motif. Dev Cell 2, 295–305.
Yu-Wai-Man P, Griffiths P, Hudson G, Chinnery PF (2009). Inherited mitochondrial optic neuropathies. J Med Genet 46, 145–158.
Zhang T, Hong WJ (2001). Ykt6 forms a SNARE complex with syntaxin 5, GS28, and Bet1 and participates in a late stage in endoplasmic reticulum-Golgi transport. Biol Chem 276, 27480–27487.
Ziegler DV, Wiley CD, Velarde MC (2015). Mitochondrial effectors of cellular senescence: beyond the free radical theory of aging. Aging Cell 14, 1–7.
Züchner S, Mersiyanova IV, Muglia M, Bissar-Tadmouri N, Rochelle J, Dadali EL, Zappia M, Nelis E, Patitucci A, Senderek J, *et al*. (2004). Mutations in the mitochondrial GTPase mitofusin 2 cause Charcot–Marie–Tooth neuropathy type 2A. Nat Genet 36, 449–451.